

## **Recurrent activating *ACVR1/ALK2* mutations in diffuse intrinsic pontine glioma**

Kathryn R Taylor<sup>1,\*</sup>, Alan Mackay<sup>1,\*</sup>, Nathalie Truffaux<sup>2</sup>, Yaron S Butterfield<sup>3</sup>, Olena Morozova<sup>4</sup>, Cathy Philippe<sup>2</sup>, David Castel<sup>2</sup>, Catherine S Grasso<sup>5</sup>, Maria Vinci<sup>1</sup>, Diana Carvalho<sup>1</sup>, Angel M Carcaboso<sup>6</sup>, Carmen de Torres<sup>6</sup>, Ofelia Cruz<sup>6</sup>, Jaume Mora<sup>6</sup>, Natacha Entz-Werle<sup>7</sup>, Wendy J Ingram<sup>8</sup>, Michelle Monje<sup>9</sup>, Darren Hargrave<sup>10</sup>, Alex N Bullock<sup>11</sup>, Stéphanie Puget<sup>12</sup>, Stephen Yip<sup>3</sup>, Chris Jones<sup>1,#</sup> & Jacques Grill<sup>2,#</sup>

<sup>1</sup>*Institute of Cancer Research, London, UK.* <sup>2</sup>*CNRS UMR 8203, Gustave Roussy, University Paris Sud, Villejuif, France.* <sup>3</sup>*BC Cancer Agency, Vancouver, Canada.* <sup>4</sup>*Biomolecular Engineering, University of California, Santa Cruz, Santa Cruz, California, USA.* <sup>5</sup>*Department of Molecular and Medical Genetics, Oregon Health and Science University, Portland, Oregon, USA.* <sup>6</sup>*Pediatric Hematology and Oncology, Hospital Sant Joan de Déu, Barcelona, Spain.* <sup>7</sup>*Centre Hospitalier Regional et Universitaire Hautepierre, Strasbourg, France.* <sup>8</sup>*Queensland Children's Tumour Bank, Queensland Children's Medical Research Institute, The University of Queensland, Brisbane, Queensland, Australia.* <sup>9</sup>*Stanford Institute for Stem Cell Biology and Regenerative Medicine, Stanford University School of Medicine, Stanford, California, USA.* <sup>10</sup>*Neuro-oncology and Experimental Therapeutics, Great Ormond Street Hospital, London, UK.* <sup>11</sup>*Structural Genomics Consortium, University of Oxford, Oxford, UK.* <sup>12</sup>*Pediatric Neurosurgery, Necker Sick Children's Hospital, Paris, France.*

*\* These authors contributed equally to this work*

*#Correspondence to:*

Chris Jones PhD FRCPATH

Glioma Team, Divisions of Molecular Pathology and Cancer Therapeutics,

The Institute of Cancer Research, Sutton, Surrey, SM2 5NG, UK

Tel: +44 20 8722 4416; Email: chris.jones@icr.ac.uk

*#Correspondence to:*

Jacques Grill MD PhD

CNRS UMR 8203 « Vectorology and Anticancer Therapeutics » and Department of Paediatric and Adolescent Oncology, Gustave Roussy Cancer Institute, Paris Sud University, 94805 Villejuif, France.

Tel: +33 142 11 62 09; Email: grill@igr.fr

*Key words:* DIPG, ACVR1/ALK2, Fibrodysplasia ossificans progressiva, BMP/TGF- $\beta$

*Running title:* ACVR1 mutations in DIPG

Diffuse intrinsic pontine gliomas (DIPGs) are highly infiltrative malignant glial neoplasms of the ventral pons that, due to their location within the brain, are unsuitable for surgical resection and consequently have a universally dismal clinical outcome. The median survival time is 9–12 months, with neither chemotherapeutic nor targeted agents showing substantial survival benefit in clinical trials in children with these tumors<sup>1</sup>. We report the identification of recurrent activating mutations in the *ACVR1* gene, which encodes a type I activin receptor serine/threonine kinase, in 21% of DIPG samples. Strikingly, these somatic mutations (encoding p.Arg206His, p.Arg258Gly, p.Gly328Glu, p.Gly328Val, p.Gly328Trp and p.Gly356Asp substitutions) have not been reported previously in cancer but are identical to mutations found in the germ line of individuals with the congenital childhood developmental disorder fibrodysplasia ossificans progressiva (FOP)<sup>2</sup> and have been shown to constitutively activate the BMP–TGF- $\beta$  signaling pathway. These mutations represent new targets for therapeutic intervention in this otherwise incurable disease.

Recent high-throughput sequencing approaches have found a striking prevalence of mutations in the genes for the histone variants H3.3 (*H3F3A*) or H3.1 (*HIST1H3B*) that encode p.Lys27Met substitutions in the childhood brain tumor DIPG<sup>3</sup>. This lysine-to-methionine substitution confers a trans-dominant ablation of global trimethylation at lysine 27 of histone H3 (H3K27me3), which likely profoundly alters gene expression through the derepression of Polycomb repressive complex 2 (PRC2) target genes<sup>4</sup>. Despite these advances in understanding of the distinct biology of these tumors<sup>1</sup>, approaches for desperately needed specific therapeutic interventions are not clear, and little has been reported of the additional mutations accompanying these changes.

We carried out whole-genome sequencing on a unique series of 20 pretreatment biopsy samples of DIPG, for which the patients underwent a safe stereotactic procedure<sup>5</sup>, and whole-exome sequencing on a further biopsy case as well as 5 samples obtained at autopsy (Supplementary Table 1). Histone H3 gene mutations encoding p.Lys27Met were observed in 23 of 26 cases (88%), comprising 15 (58%) *H3F3A* mutations and 8 (31%) *HIST1H3B* mutations (Fig. 1a). These were not found in concert with mutations in the chaperones *ATRX* or *DAXX* as has been described for supratentorial pediatric glioblastoma (pGBM)<sup>6</sup>. There was also an absence of other known glioma-related molecular abnormalities such as *IDH1*, *IDH2*, *BRAF* or *FGFR1* mutations and gene fusions. The mutational spectrum of the untreated biopsy cases was not significantly different from that of the autopsy cases ( $P > 0.05$ ; Fig. 1b), although the treatment-naive samples had a low overall mutation rate, with a mean of 14.8 somatic single-nucleotide variants (SNVs) per sample (range of 0–25), that was significantly lower than observed in the radiation-treated autopsy cases (mean = 32.0, range = 14–50;  $P = 0.004$ ,  $t$  test). Similarly, there was a significantly lower overall mutation rate in untreated samples taken at biopsy than in autopsy samples (mean of 0.76 versus 1.2 mutations per megabase;  $P = 0.023$ ,  $t$  test).

Eleven of 26 DIPGs (42%) harbored somatic *TP53* mutations, with a further 6 cases (23%) shown to have SNVs in *PPM1D*, which encodes a regulator of p38 mitogen-activated protein kinase (p38-MAPK)-p53 signaling in response to cellular stress, and an additional case with a somatic *ATM* mutation (Supplementary Fig. 1), demonstrating non-overlapping targeting of a DNA damage response pathway in 18 of 26 DIPGs (69%) (Supplementary Fig. 2). We further identified non-overlapping recurrent alterations in the phosphoinositide 3-kinase (PI3K) pathway targeting *PIK3CA*, *PIK3R1* and *PTEN* through SNVs and microdeletion (Supplementary Fig. 3), in addition to amplification of *MET* (1/26; 4%) as previously described<sup>7,8</sup> and truncating mutation of *NF1* (1/26; 4%) (Fig. 1c). We also identified new recurrent somatic mutations in *IGF2R* (2/26; 8%), although these mutations were concurrent with others in the pathway, such that their consequences are unknown. In total, 12 of 26 DIPG cases (46%) harbored some form of alteration predicted to activate the receptor tyrosine kinase (RTK)-PI3K-MAPK pathways (Supplementary Fig. 4).

Heterozygous somatic coding mutations in the *ACVR1* gene, which encodes the activin A type I receptor ALK2, were observed in 7 of 26 cases (27%) (Fig. 1c). These were restricted specifically to codons 328 (c.983G>T, p.Gly328Val, two cases; c.983G>A, p.Gly328Glu, two cases), 258 (c.772C>T, p.Arg258Gly, one case) and 356 (c.1067G>A, p.Gly356Asp, one case), all within the serine/threonine kinase domain, and 206 (c.617G>A, p.Arg206His, one case), within the glycine-serine-rich (GS) domain. Screening an extended series of 26 DIPG biopsy samples by Sanger sequencing identified further recurrences of these mutations and an additional variant at position 328 (c.982G>T, p.Gly328Trp) (Supplementary Fig. 5). Overall, we identified 11 of 52 DIPG samples (21%) harboring mutation in *ACVR1* at 4 different codons (Fig. 2a). These mutations appear highly specific to DIPG. SNVs in the *ACVR1* coding region are present in the Catalogue of Somatic Mutations in Cancer

(COSMIC) database<sup>9</sup> at an overall frequency of 20 in 5,965 (0.3%), with no individual tumor type harboring them with a frequency of greater than 2% and no mutations observed to affect any of the residues described in the present study, suggestive of a 'passenger' effect in other cancers.

*ACVR1* mutations were found to cosegregate with the less common *HIST1H3B* mutation encoding p.Lys27Met in the canonical histone H3.1 variant ( $P < 0.0001$ , Fisher's exact test) (Fig. 2b), as well as with wild-type *TP53* ( $P = 0.0103$ , Fisher's exact test). There was also an association between H3.1 alteration and chromosome 2 gain (on which *ACVR1* is found at 2q24.1;  $P = 0.0009$ , Fisher's exact test). *ACVR1* mutations seem to mark a distinct subset of DIPG cases (Supplementary Table 2). There was a marked predominance of females in the *ACVR1*-mutant tumor group compared to cases with wild-type *ACVR1* (1.75:1 versus 0.64:1 female to male ratios, respectively;  $P = 0.05$ , Fisher's exact test) (Fig. 2c), as well as a relatively restricted age of onset (Fig. 2d). Cases with tumors harboring *ACVR1* mutations also had longer overall survival times (median of 14.9 versus 10.9 months;  $P = 0.05$ , log-rank test) (Fig. 2d), although outcome remained very poor. There were no significant differences in histology between the groups (Fig. 2e). Whole-genome sequencing of biopsy samples exemplifying the genotype with concurrent *ACVR1* and *HIST1H3B* mutations harbored an additional 10–19 somatic SNVs and 0–9 structural variations (Fig. 2f).

Remarkably, these somatic mutations in *ACVR1* affected identical residues as the ones described in the germ line of individuals with the autosomal dominant congenital childhood developmental disorder FOP (MIM 135100)<sup>2</sup>. This debilitating disease is characterized by heterotopic ossification of soft connective tissue resulting in severe skeletal abnormalities<sup>10</sup>. Individuals with classical clinical features of FOP carry heterozygous mutations in *ACVR1* encoding p.Arg206His that affect the GS

activation domain<sup>11</sup>, whereas atypical cases with a less severe phenotype have been shown to harbor either mutations encoding p.Arg258Ser<sup>12</sup>, p.Gly328Glu, p.Gly328Arg or p.Gly328Trp<sup>13</sup> or p.Gly356Asp<sup>14</sup> or other heterozygous mutations affecting the GS and kinase domains<sup>2,15</sup>. This latter series of alterations may be exposed to be present at the interface with the GS domain and may abrogate interactions with the negative regulator FKBP12 (refs. 12,13,15). These mutations have been shown to constitutively activate the bone morphogenetic protein (BMP)-dependent transforming growth factor (TGF)- $\beta$  pathway in the absence of ligand binding, as evidenced by increased phosphorylation of SMAD1, SMAD5 and SMAD8 (SMAD1/5/8) in vitro<sup>14,16</sup>.

To investigate the specific role of *ACVR1* mutations in the context of DIPG, we assembled a panel of four DIPG case-derived primary cultures (and one thalamic pediatric GBM (glioblastoma multiforme) culture harboring an *H3F3A* mutation encoding p.Lys27Met), representing two *ACVR1* mutations (encoding p.Arg206His and p.Gly328Val) and three wild-type lines (Supplementary Table 3). In these models, RNA sequencing (RNA-seq) data demonstrated that the mutant allele was expressed in approximately half of the reads, which was also evidenced by Sanger sequencing of cDNA from case sample NCHP\_DIPG011 (Supplementary Fig. 6). Treatment with the selective ALK2 inhibitor LDN-193189 (ref. 17) resulted in marked inhibition of cell viability in all cells, with GI<sub>50</sub> values (concentrations required to inhibit cell growth by 50%) ranging from 0.86–2.1  $\mu$ M, approximately tenfold lower than with the less potent parent compound dorsomorphin, with a trend toward increased sensitivity in the mutant cultures ( $P = 0.10$ , F test) (Fig. 3a). Transfection of thalamic GBM and DIPG cells with wild-type *ACVR1* (both with *H3F3A* mutation encoding p.Lys27Met) with constructs encoding Flag-tagged mutants conferred increased signaling through phosphorylated SMAD1/5/8, particularly for the Arg206His mutant and, to a lesser extent, for the Gly328Glu mutant (Fig. 3b). *ACVR1* mutation may

only be one mechanism by which this pathway is activated in DIPG, however, as high basal levels of phosphorylated SMAD1/5/8 were also observed for the cells with *H3F3A* mutation encoding p.Lys27Met and wild-type *ACVR1* that were used in this study (Supplementary Fig. 7). This finding may explain the lack of a more robust genotype-dependent response to the inhibitor and may also expand the population of patients who might benefit from targeting of the receptor.

There are no reports to our knowledge of coincident FOP and DIPG, although the clinical features of both typical and atypical cases of FOP can commonly include neurological symptoms and have been reported in children to include cerebellar and brain stem abnormalities<sup>15,18</sup>, including demyelinated lesions in the pons, both in human cases and mouse models<sup>19</sup>. It will nonetheless be a challenge to identify the mechanism by which the temporal and spatial context of BMP–TGF- $\beta$  pathway activation confers such differing clinical phenotypes. In experimental models of FOP, *ACVR1* mutations are associated with defects in stem cell maintenance, reprogramming and differentiation, offering links with cancer-related cellular processes. First-generation ALK2 inhibitors such as dorsomorphin<sup>20</sup> and LDN-193189 (ref. 17) have been shown to downregulate intracellular BMP–TGF- $\beta$  signaling and to reduce heterotypic ossification, opening the tantalizing possibility of central nervous system (CNS)-penetrant compounds showing a similar potential in a childhood brain tumor otherwise devoid of efficacious treatment options.

## LEGENDS FOR FIGURES

**Figure 1 – Genomic landscape of DIPG.** (a) Pie chart showing breakdown of histone H3 mutations in our series of 26 DIPG samples (*H3F3A* mutation encoding p.Lys27Met: 15/26, 58%; *HIST1H3B* mutation encoding p.Lys27Met: 8/26, 31%, wild-type histone H3: 3/26, 11%). (b) Mutational spectrum of DIPG. Bar chart showing the total number of somatic coding variants, coding SNVs, indels, amplifications, deletions and structural variations for each DIPG case. Biopsy cases are marked by the dark brown bar along the x axis, and autopsy cases are marked by the light brown bar. (c) Summary of major alterations found. Clinicopathological information for the 26 DIPG samples is provided along with the mutation rate and number of somatic coding SNVs. Mutations, amplifications and deletions are noted for the histone H3 genes and *ATRX* or *DAXX*, *ACVR1*, the *ATM-TP53-PPM1D* axis, members of the PI3K-MAPK signaling pathways, RTKs and members of the RB pathway as are chromosome 1q and 2 single-copy gains and amplification (amp) of *MYC* or *MYCN*. GBM, glioblastoma multiforme; AA, anaplastic astrocytoma; AOA, anaplastic oligoastrocytoma; LGA, low-grade astrocytoma; M, male; F, female.

**Figure 2 – Recurrent activating *ACVR1/ALK2* mutations in DIPG.** (a) Schematic showing recurrent missense mutations in *ACVR1*, overlaid with functional protein domains and exon boundaries. In total, 11 of 52 DIPGs (21%) harbored somatic alterations at 4 residues, all of which have previously been described in the germ line of individuals with FOP. Specific base changes that may be unique to DIPG are highlighted in bold. Activin, activin type I and II receptor domain; GS, TGF- $\beta$  glycine-serine-rich domain; PKc, protein kinase catalytic domain; PKc\_like, protein kinase catalytic domain like. (b) Bar graphs showing segregation of activating mutations in *ACVR1* with *HIST1H3B* mutations encoding p.Lys27Met ( $P < 0.0001$ , Fisher's exact test) and with wild-type (WT) *TP53* ( $P = 0.0103$ , Fisher's exact test) in our extended

series of 52 DIPG cases. (c) Sex distribution of cases with *ACVR1* mutations, showing a strong predominance of females in mutant samples. (d) Age distribution (left) and overall survival (right) of DIPG cases with *ACVR1* mutations compared to cases with wild-type *ACVR1*. (e) Bar plots representing the histological breakdown of samples with mutant and wild-type *ACVR1*. Brown, World Health Organization (WHO) grade 4; orange, WHO grade 3; tan, WHO grade 2. (f) Circos plots representing the whole-genome sequences of the four DIPG cases with concurrent *ACVR1* mutation, *HIST1H3B* mutation encoding p.Lys27Met and wild-type *TP53*. The outer ring contains chromosomal ideograms, annotated for somatic SNVs in coding genes. The middle ring plots copy number derived from coverage data: dark red, amplification; pink, gain; dark blue, deletion; light blue, loss. The inner ring represents loss of heterozygosity (LOH; yellow). Drawn inside the circle are structural variations: red, interchromosomal translocation; blue, intrachromosomal translocation; orange, deletion; purple, inversion.

**Figure 3** – *ACVR1* mutations are weakly activating and responsive to targeted inhibition. (a) In vitro cytotoxicity of the ALK2 inhibitor LDN-193189. Primary cultures were treated with inhibitor for 72 h, and cell viability was measured by CellTiter-Glo in triplicate experiments. Error bars, s.d. The cells used were HSJD-DIPG007 (DIPG; *ACVR1* Arg206His, *H3F3A* Lys27Met), SU-DIPG-IV (DIPG; *ACVR1* Gly328Val, *HIST1H3B* Lys27Met), CHRU-TC68 (DIPG; *ACVR1* wild type, *H3F3A* Lys27Met), SU-DIPG-VI (DIPG; *ACVR1* wild type, *H3F3A* Lys27Met) and QCTB-R059 (thalamic pediatric GBM; *ACVR1* wild type, *H3F3A* Lys27Met). (b) *ACVR1* mutations confer increased signaling through phosphorylated SMAD1/5/8. QCTB-R059 and SU-DIPG-VI cells were transfected with construct encoding Flag-tagged Arg206His or Gly328Glu mutant ALK2 and assessed for phosphorylated SMAD1/5/8 (p-SMAD1/5/8) by protein blot. EV, empty vector; WT, wild-type ALK2.  $\alpha$ -tubulin is included as a loading control. Numbers below each lane represent phosphorylated SMAD1/5/8 levels quantified relative to the levels of Flag expression.

## **ACKNOWLEDGEMENTS**

This study was funded by the Cancer Research UK Genomics Initiative (A14078) and makes use of data generated by the St. Jude Children's Research Hospital–Washington University Pediatric Cancer Genome Project. We are grateful to the DIPG Preclinical Consortium funded by The Cure Starts Now and the Lyla Nsouli Foundation for RNA-seq data. This work is supported by the Stavros Niarchos Foundation, Abbie's Army, the Lyla Nsouli Foundation, the Royal Marsden Hospital Children's Department Fund and Fondo Alicia Pueyo. M.M. gratefully acknowledges funding by the National Institutes of Neurological Disease and Stroke (NINDS; grant K08NS070926), Alex's Lemonade Stand Foundation, the McKenna Claire Foundation and the Dylan Jewett, Elizabeth Stein, Connor Johnson and Zoey Ganesh Memorial Funds. C.P. acknowledges funding from the Agence National de la Recherche. N.T., C.P. and J.G. acknowledge funding from the charity l'Etoile de Martin, and N.E.-W. acknowledges support from Enfants et Santé. A.M.C. acknowledges funding from the Fundación Científica de la Asociación Española Contra el Cáncer. W.J.I. acknowledges funding from the Children's Health Foundation Queensland and the Brainchild Foundation. The Structural Genomics Consortium is a registered charity (1097737) that receives funds from AbbVie, Boehringer Ingelheim, the Canada Foundation for Innovation, the Canadian Institutes for Health Research, Genome Canada, GlaxoSmithKline, Janssen, Lilly Canada, the Novartis Research Foundation, the Ontario Ministry of Economic Development and Innovation, Pfizer, Takeda and the Wellcome Trust (092809/Z/10/Z). K.R.T., A.M., M.V., D. Carvalho, D.H. and C.J. acknowledge National Health Service (NHS) funding to the National Institute of Health Research Biomedical Research Centres.

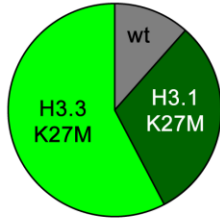
## REFERENCES

1. Jones, C., Perryman, L. & Hargrave, D. Paediatric and adult malignant glioma: close relatives or distant cousins? *Nat. Rev. Clin. Oncol.* **9**, 400–413 (2012).
2. Katagiri, T. Recent topics in fibrodysplasia ossificans progressiva. *J. Oral Biosciences* **54**, 119–123 (2012).
3. Wu, G. *et al.* Somatic histone H3 alterations in pediatric diffuse intrinsic pontine gliomas and non-brainstem glioblastomas. *Nat. Genet.* **44**, 251–253 (2012).
4. Lewis, P.W. *et al.* Inhibition of PRC2 activity by a gain-of-function H3 H3 mutation found in pediatric glioblastoma. *Science* **340**, 857–861 (2013).
5. Roujeau, T. *et al.* Stereotactic biopsy of diffuse pontine lesions in children. *J. Neurosurg.* **107**, 1–4 (2007).
6. Schwartzentruber, J. *et al.* Driver mutations in histone H3.3 and chromatin remodelling genes in paediatric glioblastoma. *Nature* **482**, 226–231 (2012).
7. Puget, S. *et al.* Mesenchymal transition and PDGFRA amplification/mutation are key distinct oncogenic events in pediatric diffuse intrinsic pontine gliomas. *PLoS ONE* **7**, e30313 (2012).
8. Paugh, B.S. *et al.* Genome-wide analyses identify recurrent amplifications of receptor tyrosine kinases and cell-cycle regulatory genes in diffuse intrinsic pontine glioma. *J. Clin. Oncol.* **29**, 3999–4006 (2011).
9. Forbes, S.A. *et al.* COSMIC: mining complete cancer genomes in the Catalogue of Somatic Mutations in Cancer. *Nucleic Acids Res.* **39**, D945–D950 (2011).
10. Shore, E.M. & Kaplan, F.S. Inherited human diseases of heterotopic bone formation. *Nat. Rev. Rheumatol.* **6**, 518–527 (2010).
11. Shore, E.M. *et al.* A recurrent mutation in the BMP type I receptor ACVR1 causes inherited and sporadic fibrodysplasia ossificans progressiva. *Nat. Genet.* **38**, 525–527 (2006).
12. Bocciardi, R., Bordo, D., Di Duca, M., Di Rocco, M. & Ravazzolo, R. Mutational analysis of the ACVR1 gene in Italian patients affected with fibrodysplasia ossificans progressiva: confirmations and advancements. *Eur. J. Hum. Genet.* **17**, 311–318 (2009).

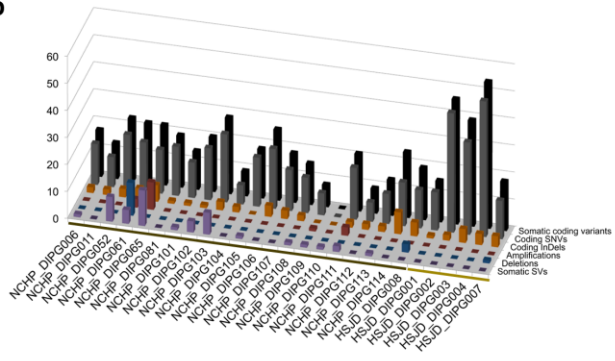
13. Petrie, K.A. *et al.* Novel mutations in ACVR1 result in atypical features in two fibrodysplasia ossificans progressiva patients. *PLoS ONE* **4**, e5005 (2009).
14. Fukuda, T. *et al.* A unique mutation of ALK2, G356D, found in a patient with fibrodysplasia ossificans progressiva is a moderately activated BMP type I receptor. *Biochem. Biophys. Res. Commun.* **377**, 905–909 (2008).
15. Kaplan, F.S. *et al.* Classic and atypical fibrodysplasia ossificans progressiva (FOP) phenotypes are caused by mutations in the bone morphogenetic protein (BMP) type I receptor ACVR1. *Hum. Mutat.* **30**, 379–390 (2009).
16. Chaikuad, A. *et al.* Structure of the bone morphogenetic protein receptor ALK2 and implications for fibrodysplasia ossificans progressiva. *J. Biol. Chem.* **287**, 36990–36998 (2012).
17. Yu, P.B. *et al.* BMP type I receptor inhibition reduces heterotopic ossification. *Nat. Med.* **14**, 1363–1369 (2008).
18. Tumolo, M., Moscatelli, A. & Silvestri, G. Anaesthetic management of a child with fibrodysplasia ossificans progressiva. *Br. J. Anaesth.* **97**, 701–703 (2006).
19. Kan, L. *et al.* CNS demyelination in fibrodysplasia ossificans progressiva. *J. Neurol.* **259**, 2644–2655 (2012).
20. Yu, P.B. *et al.* Dorsomorphin inhibits BMP signals required for embryogenesis and iron metabolism. *Nat. Chem. Biol.* **4**, 33–41 (2008).

**Figure 1**

**a**



**b**



**c**

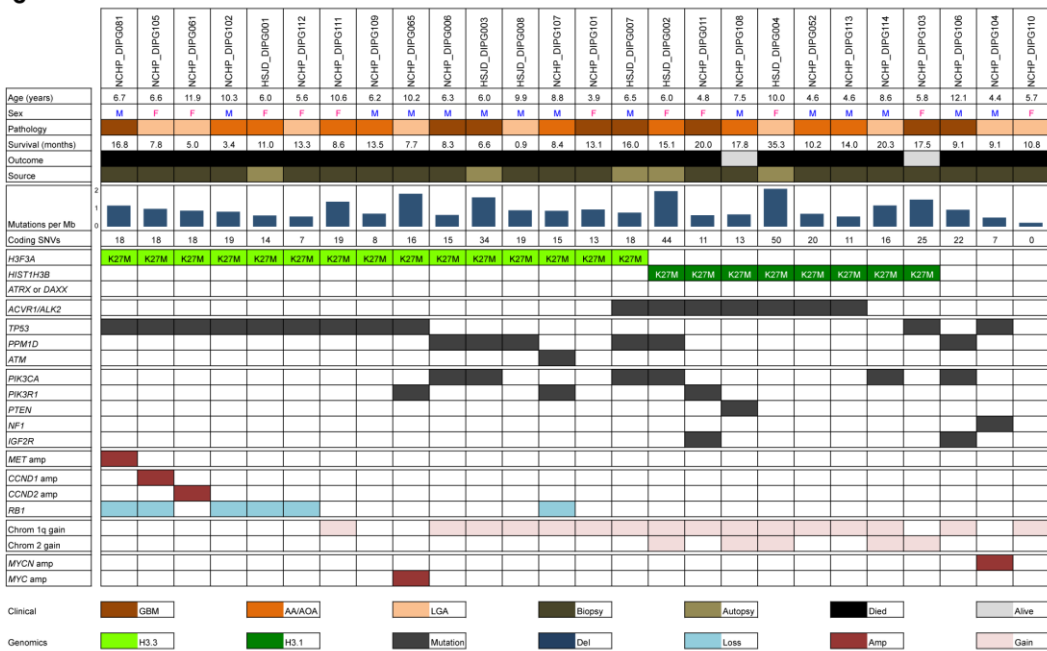


**Figure 2**

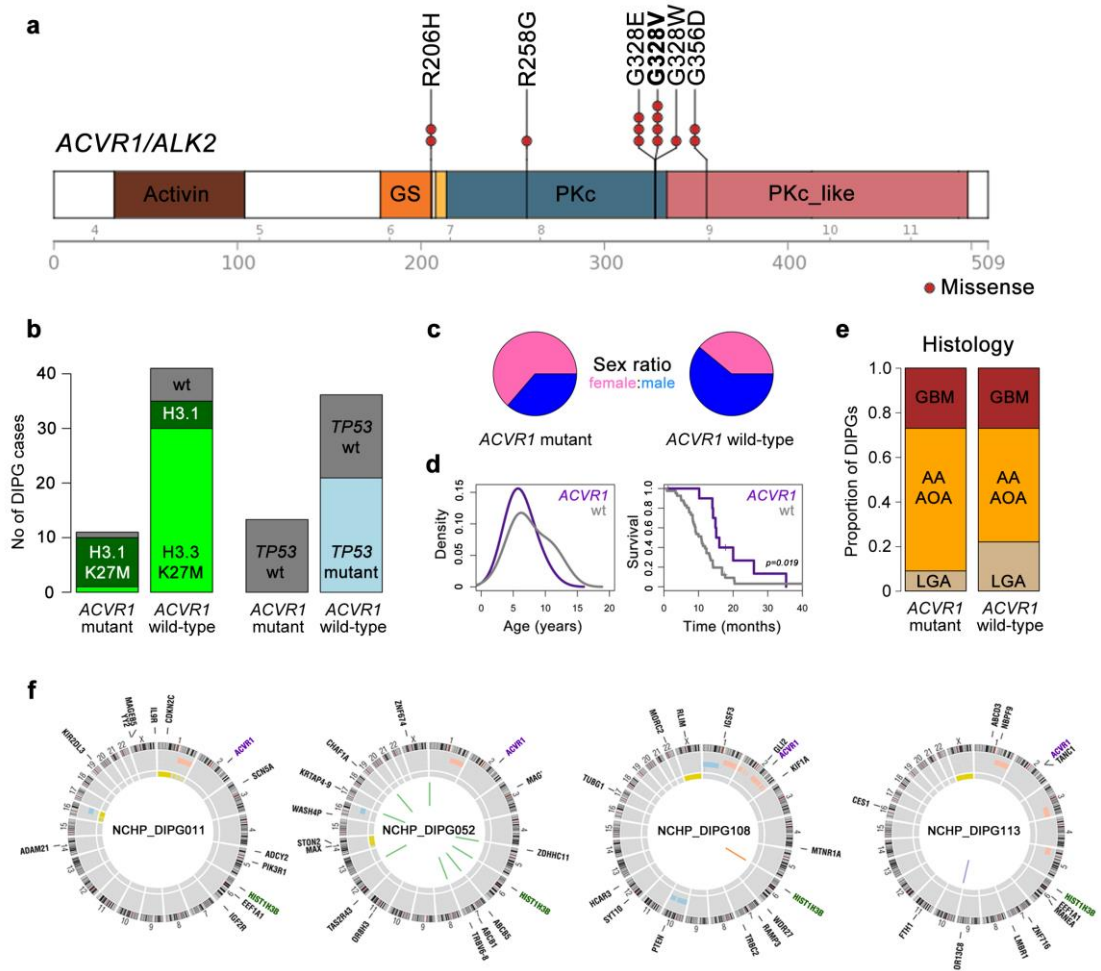
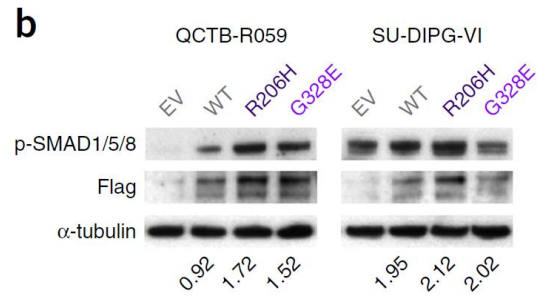
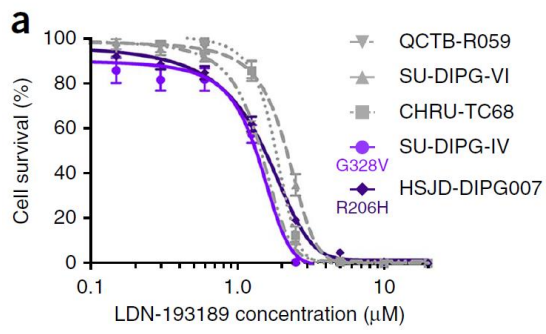


**Figure 3**



## SUPPLEMENTARY METHODS

### Tumour cohort

DIPG samples and matched peripheral blood samples were available from 21 patients who underwent stereotactic biopsy at the Neurosurgery Department of Necker Sick Children's Hospital (Paris, France), 20 of which were subjected to whole-genome sequencing. All patients were clinically diagnosed as having DIPG on the basis of clinical presentation and radiography as part of a multidisciplinary assessment. These patients had diffuse intrinsic tumor centered in the pons and occupying at least 50% of the volume of this structure and had an associated short clinical history of less than 3 months. DNA from an additional 26 biopsy samples was available as a validation cohort. A further five DIPG cases with matched peripheral blood samples were obtained at autopsy at the Hospital Sant Joan de Déu (Barcelona, Spain) and were sequenced after exome capture using Agilent SureSelect technology. All patient material was collected after informed consent and was subject to local research ethics committee approval. Cases included 23 girls and 29 boys (1:1.26 ratio). The median age of the patients was 6.6 years, and the median overall survival time was 11.6 months. A summary of the tumor cohort and clinicopathological information are provided in Supplementary Table 2.

### Whole genome / exome sequencing

Exome capture was carried out on the four autopsy cases using the 50Mb Agilent SureSelect platform (Agilent Technologies), and samples underwent paired-end sequencing on an Illumina HiSeq 2000 with a 100-bp read length. Library preparation for the biopsy samples was carried out by the Illumina FastTrack service, and entire genomes underwent paired-end sequencing on an Illumina HiSeq 2000. The median coverage for the tumor genomes was 37–67× (matched normal genomes, 34–41×). Reads were mapped to the hg19 build of the human genome using BWA (Burrows-Wheeler Aligner), and PCR duplicates were removed with PicardTools 1.5.

## Genome analysis

Somatic SNVs were called using the Illumina Genome Network (IGN) Cancer Normal pipeline version 1.0.2 and the Genome Analysis Toolkit v2.4-9. Structural variations were called using IGN and SVDetect. Variants were annotated using the Ensembl Variant Effect Predictor v71 tool incorporating SIFT and PolyPhen predictions, COSMIC v64 and dbSNP Build 137 annotations. Copy number was obtained by calculating log<sub>2</sub> ratios of tumor/normal coverage binned into exons of known genes, smoothed using circular binary segmentation and processed using in-house scripts. LOH was calculated using APOLLOH. Schematics showing the locations of recurrent mutations were produced by the St. Jude Washington University Protein Paint tool. Statistical analysis was carried out using R3.0.1. Continuous variables were analyzed using Student's t tests. Count data were compared using Fisher's exact test.

## Cell culture and drug sensitivity

Primary cultures were derived from DIPG patient samples taken at either biopsy or autopsy at multiple centres, representing both cases with mutant and wild-type *ACVR1* and with both *H3F3A* and *HIST1H3B* mutations encoding p.Lys27Met, in addition to cells from a pediatric glioblastoma specimen arising in the thalamus with an *H3F3A* mutation encoding p.Lys27Met. A summary of the cases from which these cells were derived is provided in Supplementary Table 3. Cells were grown under adherent stem cell conditions using flasks coated with laminin (Sigma) in neurobasal medium (Invitrogen) supplemented with B-27 (Invitrogen) and the growth factors epidermal growth factor (EGF), basal fibroblast growth factor (bFGF), platelet-derived growth factor (PDGF)-AA and PDGF-BB (all from Shenandoah Biotech). The ALK2 inhibitors LDN-193189 (Sigma) and dorsomorphin (Abcam) were tested for their effects on cell viability using a highly sensitive luminescent assay measuring cellular ATP levels (CellTiter-Glo, Promega). Drug was added in various concentrations, and cells were assayed in triplicate after 72 h. Statistical analysis was carried out using GraphPad Prism 6.0 (GraphPad Software).

#### Allelic expression of ACVR1.

SU-DIPG-IV cells were subjected to full transcriptome sequencing as part of the DIPG Preclinical Consortium. Counts of reads aligned to the *ACVR1* coding region in NCBI\_36 were analyzed for the ratio of mutant to wild-type sequence and visualized in Genome Browse (Golden Helix). RNA from the NCHP\_DIPG011 primary tumor was reverse transcribed, PCR amplified and underwent Sanger sequencing to determine whether both mutant and wild-type alleles were expressed (Supplementary Table 4).

#### Overexpression of mutant ALK2

The *ACVR1* mutations encoding p.Arg206His and p.Gly328Glu were introduced into pcDNA3.1 by site-directed mutagenesis as previously described<sup>16</sup>, and constructs were transfected into primary QCTB-R059 and SU-DIPG-VI cells using Lipofectamine (Invitrogen), with protein collected after 24 h using standard procedures. Protein blotting was carried out with horseradish peroxidase (HRP)-conjugated antibody to Flag (A8592, Sigma; 1:1,000 dilution) and antibody to phosphorylated SMAD1/5/8 (9511, Cell Signaling Technology; 1:1,000 dilution) under standard conditions. Relative levels of phosphorylated SMAD1/5/8 were measured with ImageJ software (National Institute of Mental Health).

#### Statistical analysis

Statistical analysis was carried out using GraphPad Prism 6.0 and R 3.0.1. Comparisons of the numbers of coding SNVs and the mutation rates in biopsy and autopsy cases were performed by t test. For analysis of categorical association between cases with *ACVR1* mutations and mutations in *HIST1H3B* or *TP53*, sex and histology, Fisher's exact test was used. Differences in survival were analyzed by the Kaplan-Meier method, and significance was determined by the log-rank test. All tests were two-sided, and a *P* value of less than 0.05 was considered significant. A sum-of-squares F test was used to assess differences in dose response curves for *ACVR1*-mutant versus wild-type cells.

## LEGENDS FOR SUPPLEMENTARY FIGURES

### **Supplementary Figure S1** – *Somatic mutations in TP53, PPM1D and ATM in DIPG.*

Cartoon showing recurrent and non-overlapping missense and frameshift mutations in TP53 (11/26, 42%), PPM1D (6/26, 23%) and ATM (1/26, 4%), overlaid with functional protein domains and exon boundaries. TAD: p53 transactivation motif; DNA binding: p53 DNA-binding domain; PP2C: protein phosphatase 2C domain; PP2Cc: Serine/threonine phosphatase, family 2C, catalytic domain. TAN: telomere length maintenance and DNA damage repair domain; FAT: FRAP, ATM and TRRAP associated domain; PI3Kc: phosphoinositide 3-kinase class I catalytic domain.

### **Supplementary Figure S2** – *Pathway-level recurrence of somatic alterations*

*involved DNA damage response.* Cartoon representing the frequency of distinct non-overlapping hits in intracellular components of ATM/p53-mediated DNA damage and stress response signalling. Bars are coloured according to frequency of alterations in the present cohort: red=gain of function, blue=loss of function. In total, 18/26 (69%) cases harboured alteration at some point in the pathway which would be predicted to be activating.

### **Supplementary Figure S3** – *Somatic mutations in genes involved in PI3K/MAPK*

*signalling in DIPG.* Cartoon showing non-overlapping missense, nonsense truncating mutations, and deletions in *PIK3CA* (6/26,23%), *PIK3R1* (3/26, 12%), *PTEN* (1/26, 4%) and *NF1* (1/26, 4%), overlaid with functional protein domains and exon boundaries. There were additional novel somatic mutations of unknown significance identified in *IGF2R*. Grey bars = deletions. p85B: p85 binding domain; RBD: Ras binding domain; C2 PI3K 1a: C2 domain present in class I alpha PI3 kinases; PI3Ka:

PI3K class I accessory domain; PI3Kc: PI3K class I catalytic domain; SH: Src homology domain; RhoGAP: GTPase activator protein for Rho-like GTPases domain; COG4942: Membrane-bound metallopeptidase domain; PTPc: Protein tyrosine phosphatase, catalytic domain; PTEN\_C2: PTEN C terminal 2 domain; RasGAP: Ras GTPase activating protein domain; SEC14: Sec14p-like lipid binding domain. CIMR: cationindependent mannose-6-phosphate receptor repeat; FN2: fibronectin type II domain.

**Supplementary Figure S4** – *Pathway-level recurrence of somatic alterations*

*involved in RTK / PI3K / MAPK signalling.* Cartoon representing the frequency of distinct non-overlapping hits in intracellular components of PI3K/MAPK pathway signalling, as well as amplifications of receptor tyrosine kinases, in DIPG. Bars are coloured according to frequency of alterations in the present cohort: red=gain of function, blue=loss of function. IGF2R binds IGF2 ligand preventing signalling through IGF1R/PI3K, and is found to have a somatic missense K162R and D1830E mutations. In total, 12/26 (46%) cases harboured alteration at some point in the pathway which would be predicted to be activating.

**Supplementary Figure S5** – *Sanger sequencing validation of ACVR1/ALK2*

*mutations in an extended cohort of DIPG.* Sequence traces of heterozygous mutations in the activin A type I receptor (*ACVR1/ALK2*) observed in a series of 50 DIPG, including (a) c.617G>A, R206H; (b) c.983G>A, p.G328E; (c) c.983G>T, p.G328V; (d) c.982G>T, p.G328W. All are reported to be constitutively activating of the BMP/TGF- $\beta$  signalling pathway in models of fibrodysplasia ossificans progressiva.

**Supplementary Figure S6 – Allele-specific expression of ACVR1/ALK2 mutation.** (a)

Pile-up of sequence reads from RNAseq data of SU-DIPG-IV cells, showing expression of both the wild-type and mutant alleles at position chr2:158330762, with 49/83 reads harbouring the C>A (c.983G>T) mutation (red) corresponding to ACVR1/ALK2 p.G328V. (b) Sanger sequencing of an ACVR1/ALK2 exon 8 RT-PCR product from DIPG patient sample NCHP\_DIPG011, showing heterozygous expression of the mutant p.G328E allele (c.983G>A), forward and reverse.

**Supplementary Figure S7 – Basal levels of phospho-Smad 1/5/8 in DIPG cells.**

Western blot analysis of phospho-Smad 1/5/8 (lower band) in SU-DIPG-IV (DIPG, ACVR1/ALK2 G328V, HIST1H3B K27M), HSJD-DIPG007 (DIPG, ACVR1/ALK2 R206H, H3F3A K27M), SU-DIPGVI (DIPG, ACVR1/ALK2 wt, H3F3A K27M), CHRUTC68 (DIPG, ACVR1/ALK2 wt, H3F3A K27M) and QCTB-R059 (thalamic paediatric GBM, ACVR1/ALK2 wt, H3F3A K27M).  $\alpha$ -tubulin is included as a loading control.

**Supplementary Table S2 – Description of samples used in this study.**

Clinicopathological annotation of the 26 DIPG cases profiled by whole genome or exome sequencing in this study, as well as those used in the validation cohort. DIPG: diffuse intrinsic pontine glioma; GBM: glioblastoma multiforme; AA: anaplastic astrocytoma; AOA: anaplastic oligoastrocytoma; LGA: low grade astrocytoma. WGS: whole genome sequencing; WES: whole exome sequencing; VAL: validation.

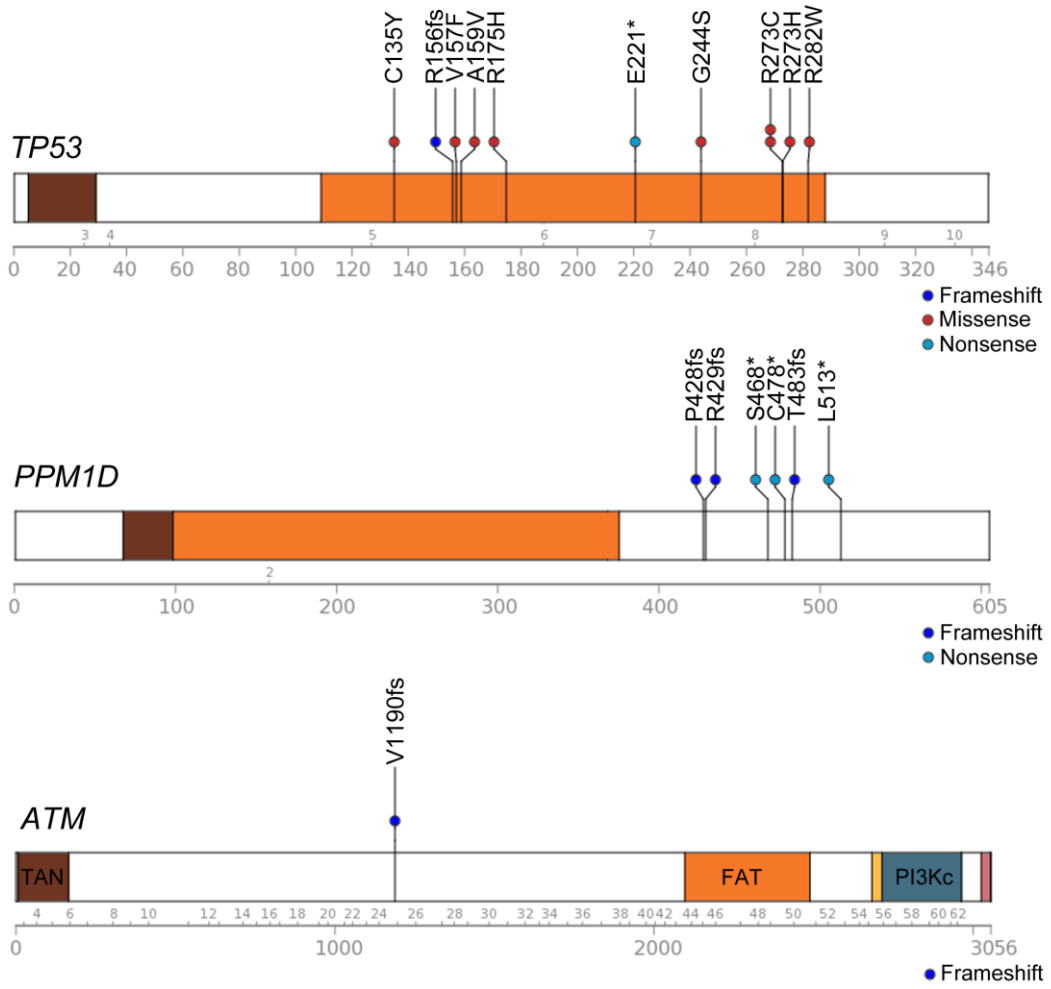
**Supplementary Table S3 – Details of primary cell cultures used.** Clinical and

molecular data relating to the four DIPG and one H3F3A K27M mutant thalamic paediatric GBM cell cultures used for preclinical and mechanistic studies. DIPG:

diffuse intrinsic pontine glioma; GBM: glioblastoma multiforme; AA: anaplastic astrocytoma.

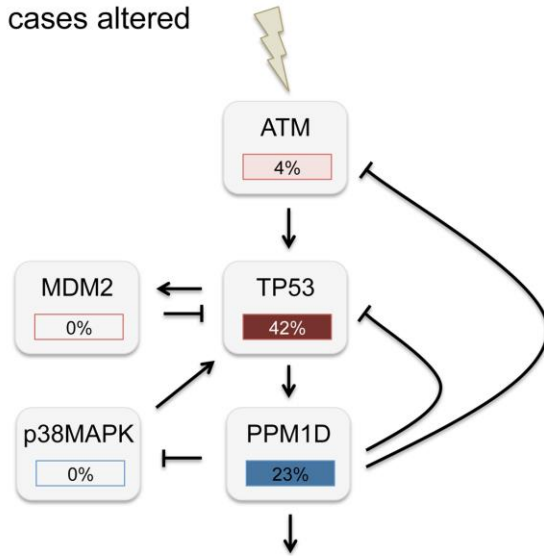
**Supplementary Table S4** – *PCR primers used*. Sequences are given for PCR amplification of *H3F3A*, *HIST1H3B* and *ACVR1* from genomic DNA for mutation detection, and *ACVR1* from mRNA to determine allele-specific expression of the mutant.

Supplementary Figure S1



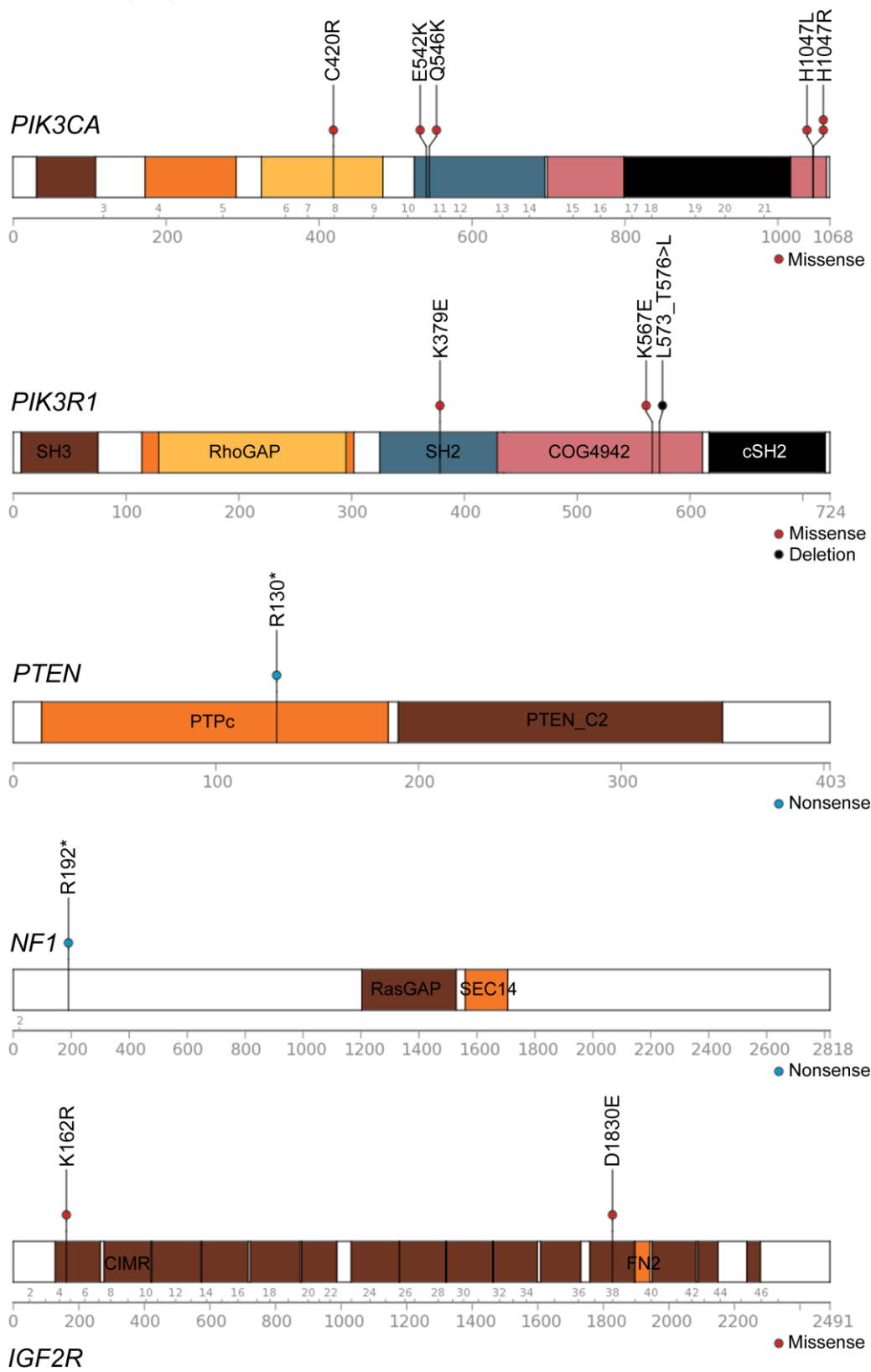
Supplementary Figure S2

DNA damage  
69% cases altered

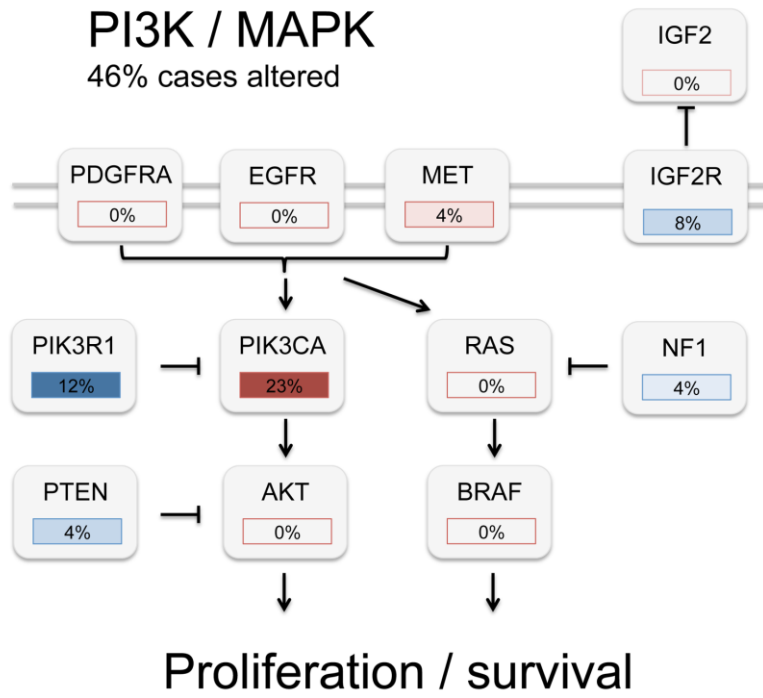


DNA repair / cell cycle arrest / apoptosis

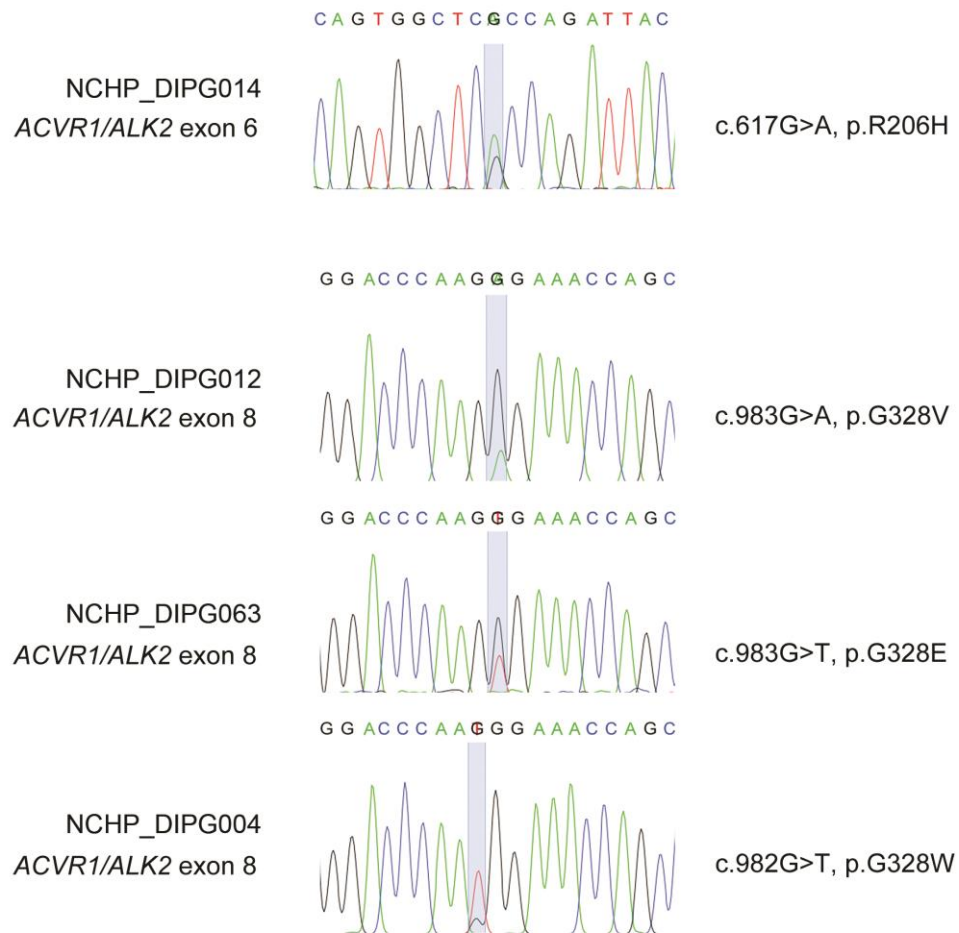
Supplementary Figure S3



Supplementary Figure S4



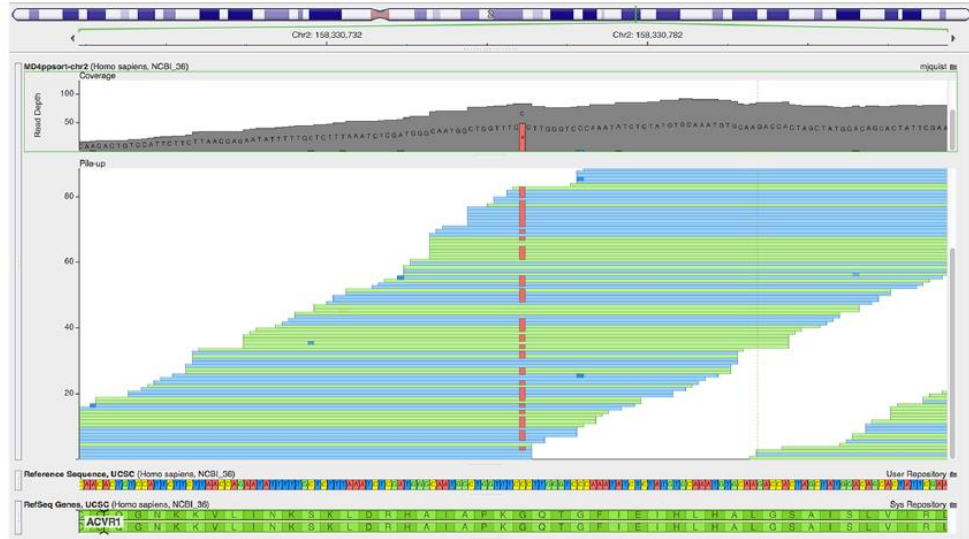
Supplementary Figure S5



# Supplementary Figure 6

**a**

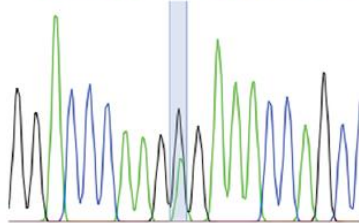
SU-DIPG-IV



**b**

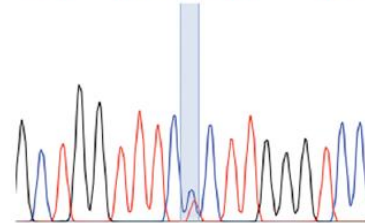
NCHP\_DIPG011

GGACCCAAAGG/A GAAACCAGC



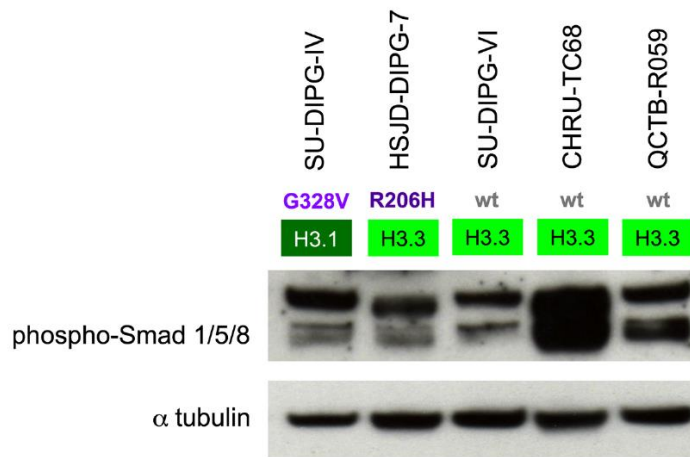
Forward cDNA sequence

GCTGGTTTC C/T CTTGGGTCC



Reverse cDNA sequence

Supplementary Figure 7



Supplementary Table 2

Study ID	Local ID	Hospital	Clinical diagnosis	Location	Age (yrs)	Sex	Histology	WHO	Source	Survival (months)	Outcome	Seq	Histone H3	ACVR1
NCHP_DIPG006	BAUK	Necker Childrens Hospital, Paris	DIPG	Pons	6.3	Male	GBM	4	Biopsy	8.3	Died	WGS	H3F3A	wt
NCHP_DIPG011	BOUC	Necker Childrens Hospital, Paris	DIPG	Pons	4.8	Female	AA	3	Biopsy	20.0	Died	WGS	HIST1H3B	G328E
NCHP_DIPG052	INAR	Necker Childrens Hospital, Paris	DIPG	Pons	4.6	Male	AA	3	Biopsy	10.2	Died	WGS	HIST1H3B	G328V
NCHP_DIPG061	MAHJ	Necker Childrens Hospital, Paris	DIPG	Pons	11.9	Female	LGA	2	Biopsy	5.0	Died	WGS	H3F3A	wt
NCHP_DIPG065	MJAY	Necker Childrens Hospital, Paris	DIPG	Pons	10.2	Male	GBM	4	Biopsy	16.8	Died	WGS	H3F3A	wt
NCHP_DIPG081	RUSL	Necker Childrens Hospital, Paris	DIPG	Pons	6.7	Male	GBM	4	Biopsy	16.8	Died	WGS	H3F3A	wt
NCHP_DIPG101	BAMN	Necker Childrens Hospital, Paris	DIPG	Pons	3.9	Female	GBM	4	Biopsy	13.1	Died	WGS	H3F3A	wt
NCHP_DIPG102	BENM	Necker Childrens Hospital, Paris	DIPG	Pons	10.3	Male	AOA	3	Biopsy	3.4	Died	WGS	H3F3A	wt
NCHP_DIPG103	DANA	Necker Childrens Hospital, Paris	DIPG	Pons	5.8	Female	GBM	4	Biopsy	17.5	Alive	WGS	HIST1H3B	wt
NCHP_DIPG104	DUJJ	Necker Childrens Hospital, Paris	DIPG	Pons	4.4	Male	LGA	2	Biopsy	9.1	Died	WGS	wt	wt
NCHP_DIPG105	GIBG	Necker Childrens Hospital, Paris	DIPG	Pons	6.6	Female	LGA	2	Biopsy	7.8	Died	WGS	H3F3A	wt
NCHP_DIPG106	HENJ	Necker Childrens Hospital, Paris	DIPG	Pons	12.1	Male	GBM	4	Biopsy	9.1	Died	WGS	wt	wt
NCHP_DIPG107	LACL	Necker Childrens Hospital, Paris	DIPG	Pons	8.8	Male	AA	3	Biopsy	8.4	Died	WGS	H3F3A	wt
NCHP_DIPG108	LEMN	Necker Childrens Hospital, Paris	DIPG	Pons	7.5	Male	AA	3	Biopsy	17.8	Alive	WGS	HIST1H3B	G328V
NCHP_DIPG109	MUCM	Necker Childrens Hospital, Paris	DIPG	Pons	6.2	Male	AOA	3	Biopsy	13.5	Died	WGS	H3F3A	wt
NCHP_DIPG110	PHIA	Necker Childrens Hospital, Paris	DIPG	Pons	5.7	Male	LGA	2	Biopsy	10.8	Died	WGS	wt	wt
NCHP_DIPG111	SCHL	Necker Childrens Hospital, Paris	DIPG	Pons	10.6	Female	AOA	3	Biopsy	8.6	Died	WGS	H3F3A	wt
NCHP_DIPG112	ZERR	Necker Childrens Hospital, Paris	DIPG	Pons	5.6	Female	LGA	2	Biopsy	13.3	Died	WGS	H3F3A	wt
NCHP_DIPG113	BLAG	Necker Childrens Hospital, Paris	DIPG	Pons	4.6	Male	AA	3	Biopsy	14.0	Died	WGS	HIST1H3B	G356D
NCHP_DIPG114	GONJ	Necker Childrens Hospital, Paris	DIPG	Pons	8.6	Male	LGA	2	Biopsy	20.3	Died	WGS	HIST1H3B	wt
HSJD_DIPG001	N06.48	Hospital Sant Joan de Déu, Barcelona	DIPG	Pons	6.0	Female	AA	3	Autopsy	11.0	Died	WES	H3F3A	wt
HSJD_DIPG002	N07.92	Hospital Sant Joan de Déu, Barcelona	DIPG	Pons	6.0	Female	AA	3	Autopsy	15.1	Died	WES	HIST1H3B	R258G
HSJD_DIPG003	N08.55	Hospital Sant Joan de Déu, Barcelona	DIPG	Pons	6.0	Male	GBM	4	Autopsy	6.6	Died	WES	H3F3A	wt
HSJD_DIPG004	N11.49	Hospital Sant Joan de Déu, Barcelona	DIPG	Pons	10.0	Female	LGA	2	Autopsy	35.3	Died	WES	HIST1H3B	G328E
HSJD_DIPG007	N12.32	Hospital Sant Joan de Déu, Barcelona	DIPG	Pons	9.9	Male	GBM	4	Biopsy	0.9	Died	WES	H3F3A	R206H
HSJD_DIPG008	HSJD-DIPG-8	Hospital Sant Joan de Déu, Barcelona	DIPG	Pons	6.5	Male	LGA	2	Autopsy	16.0	Died	WES	H3F3A	wt
NCHP_DIPG004	ADOM	Necker Childrens Hospital, Paris	DIPG	Pons	8.0	Female	LGA	3	Biopsy	26.0	Died	VAL	HIST1H3B	G328W
NCHP_DIPG008	BERG	Necker Childrens Hospital, Paris	DIPG	Pons	4.7	Male	AA	3	Biopsy	8.9	Died	VAL	H3F3A	wt
NCHP_DIPG012	BOUL	Necker Childrens Hospital, Paris	DIPG	Pons	4.5	Female	GBM	4	Biopsy	14.2	Died	VAL	HIST1H3B	G328V
NCHP_DIPG013	BOUM	Necker Childrens Hospital, Paris	DIPG	Pons	7.3	Female	AA	3	Biopsy	5.7	Died	VAL	H3F3A	wt
NCHP_DIPG014	BOUS	Necker Childrens Hospital, Paris	DIPG	Pons	6.2	Female	AA	3	Biopsy	1.2	Alive	VAL	wt	R206H
NCHP_DIPG025	CORC	Necker Childrens Hospital, Paris	DIPG	Pons	4.6	Male	AA	3	Biopsy	11.3	Died	VAL	H3F3A	wt
NCHP_DIPG026	CREA	Necker Childrens Hospital, Paris	DIPG	Pons	7.1	Male	LGA	2	Biopsy	12.3	Died	VAL	H3F3A	wt
NCHP_DIPG029	DECC	Necker Childrens Hospital, Paris	DIPG	Pons	3.4	Female	AA	3	Biopsy	14.1	Died	VAL	H3F3A	wt
NCHP_DIPG030	DECS	Necker Childrens Hospital, Paris	DIPG	Pons	13.6	Male	AA	3	Biopsy	9.3	Died	VAL	wt	wt
NCHP_DIPG032	DELT	Necker Childrens Hospital, Paris	DIPG	Pons	12.1	Male	AA	3	Biopsy	16.8	Died	VAL	H3F3A	wt
NCHP_DIPG043	GALC	Necker Childrens Hospital, Paris	DIPG	Pons	9.2	Male	AA	3	Biopsy	3.8	Died	VAL	wt	wt
NCHP_DIPG044	GALF	Necker Childrens Hospital, Paris	DIPG	Pons	9.4	Female	AA	3	Biopsy	8.3	Died	VAL	H3F3A	wt
NCHP_DIPG048	GVEE	Necker Childrens Hospital, Paris	DIPG	Pons	6.4	Female	AA	3	Biopsy	7.3	Died	VAL	HIST1H3B	wt
NCHP_DIPG050	HADZ	Necker Childrens Hospital, Paris	DIPG	Pons	6.5	Male	AA	3	Biopsy	7.2	Died	VAL	H3F3A	wt
NCHP_DIPG056	LEFL	Necker Childrens Hospital, Paris	DIPG	Pons	11.0	Male	AA	3	Biopsy	17.7	Died	VAL	H3F3A	wt
NCHP_DIPG062	MAKM	Necker Childrens Hospital, Paris	DIPG	Pons	10.8	Male	AA	3	Biopsy	12.3	Died	VAL	H3F3A	wt
NCHP_DIPG063	MAUM	Necker Childrens Hospital, Paris	DIPG	Pons	5.3	Female	GBM	4	Biopsy	14.9	Died	VAL	HIST1H3B	G328E
NCHP_DIPG069	NALF	Necker Childrens Hospital, Paris	DIPG	Pons	6.8	Female	GBM	4	Biopsy	6.0	Died	VAL	H3F3A	wt
NCHP_DIPG072	PAIC	Necker Childrens Hospital, Paris	DIPG	Pons	13.5	Female	GBM	4	Biopsy	10.9	Died	VAL	H3F3A	wt
NCHP_DIPG075	POIJ	Necker Childrens Hospital, Paris	DIPG	Pons	4.5	Female	GBM	4	Biopsy	20.4	Died	VAL	HIST1H3B	wt
NCHP_DIPG077	RAHR	Necker Childrens Hospital, Paris	DIPG	Pons	7.4	Female	AA	3	Biopsy	4.9	Died	VAL	H3F3A	wt
NCHP_DIPG079	RIER	Necker Childrens Hospital, Paris	DIPG	Pons	7.6	Male	GBM	4	Biopsy	14.1	Died	VAL	H3F3A	wt
NCHP_DIPG083	SANC	Necker Childrens Hospital, Paris	DIPG	Pons	11.3	Female	AA	3	Biopsy	14.2	Died	VAL	H3F3A	wt
NCHP_DIPG115	GREL	Necker Childrens Hospital, Paris	DIPG	Pons	1.7	Male	LGA	2	Biopsy	58.0	Died	VAL	H3F3A	wt
NCHP_DIPG116	HUPN	Necker Childrens Hospital, Paris	DIPG	Pons	4.4	Male	AOA	3	Biopsy	10.0	Died	VAL	wt	wt
NCHP_DIPG117	OWGC	Necker Childrens Hospital, Paris	DIPG	Pons	5.0	Male	AA	3	Biopsy	11.9	Died	VAL	HIST1H3B	wt

Supplementary Table 3

Cell line ID	Originator	Clinical diagnosis	Location	Age (yrs)	Sex	Histology	WHO	Source	Survival (months)	Outcome	Histone H3	ACVR1
CHRU-TC68	Centre Hospitalier Régional Universitaire, Strasbourg	DIPG	Pons	9.8	Female	AA	3	Biopsy	7.0	Alive	H3F3A	wt
HSJD-DIPG007	Hospital Sant Joan de Déu, Barcelona	DIPG	Pons	9.9	Male	GBM	4	Biopsy	0.9	Died	H3F3A	R206H
QCTB-R059	Queensland Children's Medical Research Institute, Brisbane	GBM	Thalamus	10.4	Female	GBM	4	Surgery	0.9	Died	H3F3A	wt
SU-DIPG-IV	Stanford University, California	DIPG	Pons	3.0	Female	GBM	4	Autopsy	8.0	Died	HIST1H3B	G328V
SU-DIPG-VI	Stanford University, California	DIPG	Pons	7.0	Female	GBM	4	Autopsy	6.0	Died	H3F3A	wt

Supplementary Table 4

Name	Forward	Reverse
H3F3A	GATTTGGGTAGACGTAATCTTCA	TTTCCTGTTATCCATCTTTTGT
HIST1H3B	GGGCAGGAGCCTCTCTTAAT	ACCAAGTAGGCCACCAAGC
ACVR1 exon 6	GATTGCTGCCCTTCATGTG	AAAAGCAGATTTTCCAAGTCC
ACVR1 exon 7	TAATGATGGGCTGGCTGC	AAAACGGAGAGAGCAAAGGC
ACVR1 exon 8	GATGACATTTACTGTGTAGGTCGC	GATGCAACTCACCTAACCATTTG
ACVR1 exon 9	TGGTTTAAAAATCCTTCAGCAGC	TTTTAAAGGTAGCTGGATCAAGAG
ACVR1 exon 8 mRNA	TCAGGAAGTGGCTCTGGTCT	CAAGTCCAAGGCCCAATA